Macromolecules
ARTICLE

*Macromolecules* **2010**, *43*, 4715–4726 **4715**
DOI: 10.1021/ma100071e

# Microstructure Studies of In Situ Composites Based on Polyethylene/Polyamide 12 Blends

**Nadya Dencheva,[†] Zlatan Denchev,*[,†] M. Jovita Oliveira,[†] and Sérgio. S. Funari[‡]**

[†]*I3N—Institute for Polymers and Composites, University of Minho, Campus Azurém, Guimarães 4800-058, Portugal, and* [‡]*HASYLAB at DESY, Notkestrasse 85, 22603 Hamburg, Germany*

*Received January 17, 2010; Revised Manuscript Received April 2, 2010*

ABSTRACT: This paper reports on the structure development at nanometer and micrometer scale during the preparation of microfibrilar composites (MFC) based on oriented blends of polyamide 12 (PA12) and high-density polyethylene (HDPE). The composites were prepared *in situ* by means of conventional processing techniques: extrusion blending, cold drawing and compression molding. The evolution of morphology in the unidirectionally aligned reinforcing fibrils (e.g., their visible diameters, lengths and aspect ratios) was followed during the various processing stages as a function of the blend composition by means of electron microscopy and synchrotron X-ray scattering techniques. It was demonstrated that the reinforcing fibrils comprise a PA12 core covered by a transcrystalline layer (TCL) of oriented polyethylene. A method was proposed for estimation of the thickness of that TCL. The influence of the compatibilizer content on the TCL thickness and structure as well as on the other morphological characteristics of the composites was assessed.

## Introduction

One of the main strategies in the production of reinforced polymer composites is the introduction of strong fibers into a bulk polymer matrix.[1] The *in situ* preparation of both matrix and fibrils resulted in what was called "microfibrilar composites" (MFC).[2,3] They were obtained by a combination of appropriate mechanical and thermal treatments in three processing stages, namely: (i) melt-blending of the starting neat polymers and extrusion; (ii) cold drawing of the blend; (iii) selective isotropization of the oriented blend at $T_1 < T < T_2$, where $T_1$ is the melting temperature of the lower-melting, matrix-forming component and $T_2$ is that of the higher melting one from which the reinforcing fibrils originate.[4] The MFC concept does not employ a starting nanomaterial to be blended with the matrix polymer, thus avoiding the general problems in nanocomposites technology, namely achieving proper dispersion of the reinforcing entities and not allowing their aggregation during processing.[5]

There exist several comprehensive reviews related to the processing, properties, and morphology of the MFC from different polymer blends.[6−8] In terms of composition, among the MFC containing polyolefins most studied are the poly(ethylene terephthalate) (PET) reinforced high-density polyethylene (HDPE),[9] polypropylene (PP),[10,11] and low-density polyethylene (LDPE).[12,13] Composites comprising a HDPE matrix reinforced with polyamide 12 (PA12) fibrils were obtained in semi-industrial scale with an initial characterization of the mechanical properties and morphology by means of scanning electron microscopy (SEM),[14] as well as by X-ray scattering techniques.[15] Recently, HDPE/PA6 microfibrilar composites have been prepared,[16] studying in detail their structure and its relation to the mechanical properties.[17]

The last step of the MFC's production cycle involves nonisothermal crystallization of the selectively molten matrix in the presence of the oriented and crystalline reinforcing fibrils with diameters from several hundred nanometers to several micrometers. It is well-known that under such thermal conditions heterogeneous nucleation can occur with sufficiently high density along the interphase region leading to the formation of layers of matrix material around the fiber, known as transcrystallinity (TC) or transcrystalline layers (TCL).

The number of studies on TC in conventional fiber reinforced composites is vast. In their recent review on the subject Quan et al[18] discussed a number of issues related to the formation and growth of TCL: crystallinity of the matrix, mismatch of thermal coefficients of the fiber and the matrix, epitaxy between the fiber and the matrix, surface toughness, thermal conductivity, treatment of fiber, etc. Processing conditions such as cooling rate, temperature, and interfacial stress were also found to be important. There are indications that the TC phenomenon is probably too specific for each fiber/matrix system. Nevertheless, it has been recognized that the orientation distribution of the polymer chains in the TCL will determine the nature and extent of its effect on the properties of the composite material.[19]

There exist a limited number of studies on the occurrence of transcrystallinity in MFC. Li et al.[11,20,21] studied the crystal morphology of PET/iPP *in situ* MFC, prepared by a slit extrusion-hot stretching-quenching process, and found that transcrystallinity occurred around the PET *in situ* microfibrils. The authors propose different nucleation mechanisms related to the external field applied to explain this form of crystallization. MFC obtained *in situ* from LDPE matrix reinforced by PET microfibrils (PET/LDPE = 1:1)[22] were injection molded and the formation of transcrystalline layers of LDPE matrix on the surface of the PET microfibrils observed by transmission electron microscopy (TEM). In these layers the crystalline lamellae were aligned parallel to each other and were placed perpendicularly to the fibril surfaces. An interesting observation was made in PET/PA12 MFC.[23,24] The PET microfibrils were not only effective nuclei for the PA12 molecules, but also caused their reorientation by 90° with respect to their initial direction: from parallel to the

*Author to whom correspondence should be addressed.


Published on Web 04/22/2010

**Table 1. Characteristics of the Materials Used**[a]

| polymer type (abbreviation in text) | trade name (manufacturer) | characteristics |
|---|---|---|
| high density polyethylene (HDPE), grade for monofilament production | VS4531 (Borealis) | density = 0.952 g/cm$^3$; MFR = 0.6 g/10 min (2.16 kg/190 °C); $\overline{M}_n \approx 49761$; $\overline{M}_w = 203120$; $\overline{M}_E = 1089000$ (g/mol); PD = 4.1; Iv = 1.275 dL/g;[b] melting point = 133 °C (DSC) |
| polyamide 12, high viscosity grade (PA12) | Grilamid L 25 (EMS GRIVORI) | density = 1.01 g/cm$^3$; MVR = 20 cm$^3$/10 min (5 kg/275 °C); $\overline{M}_n = 73300$; $\overline{M}_w = 131900$ g/mol; PD = 1.8;[c] melting point = 178 °C (DSC) |
| modified linear low density PE (YP) | Yparex 8102 (DSM) | density = 0.923 g/cm$^3$; MFR = 2.3 g/10 min (2.16 kg/190 °C); $\overline{M}_n = 31984$; $\overline{M}_w = 195657$; $\overline{M}_z = 792342$ (g/mol); PD ≈ 6.1; Iv = 0.780 dL/g;[b] % bound MAH = 0.5 −1.0% wt;[d] melting point = 125 °C (DSC) |

[a] Key: MFR = melt mass flow rate; PD = $M_w/M_n$, polydispersity; MVR = melt volume rate (ISO 1133); Iv = intrinsic viscosity. [b] The average molecular weights, the PD and Iv values for HDPE and YP were obtained in a Viscotek GPC/SEC system model 350 with triple detection−refractive index (RI), viscosimetry and light scattering, operating at 154 °C with *o*-dichlobenzene as a solvent. Three Vicotek special application columns (30 cm long) were used packed with fluorinated, highly crossed-linked divinyl-benzene gel with exclusion limits of >10K, > 20K, and >200K ($M_w$, g/mol), respectively. [c] Equipment: Waters 150 with RI detection, 2 columns (30 cm long) with PL mixed B gel packing operating at 130 °C with benzyl alcohol solvent. [d] Based on FT-IR data. Equipment: Perkin-Elmer Spotlight 300 system; thin films obtained by compression molding studied in transmission mode. For details, see the text.

main chain direction of PET macromolecules in the oriented precursor to perpendicular in the MFC.

It can be concluded that although transcrystallization is observed in some MFC systems, as yet this phenomenon is far from being completely understood. As MFC belong to the fiber-reinforced composites, their mechanical properties will be expected to depend on the effectiveness of the transfer of stress between the fiber and matrix,[25] i.e., on the structure and thickness of the TCL.

In this study by means of a combination of SEM and synchrotron X-ray scattering techniques we study the development of morphology and microstructure in a series of HDPE/PA12 oriented blends with different composition during their processing to MFC with unidirectional orientation of the reinforcing fibrils. It was found that these are covered by a transcrystalline layer of oriented HDPE matrix material. An attempt was made to estimate the thickness of this layer and to create a model adequately explaining the structural data of PA12-reinforced MFC. In doing so, structural information about oriented and isotropic neat PA12 was used, which was obtained previously under conditions similar to those of the MFC preparation.[26,27]

## Experimental Section

**Materials.** Table 1 summarizes the properties of the starting materials used in the study. As they are all commercial products, care was taken for their detailed characterization in terms of molecular weights and chemical composition. Such information is typically not provided by the manufacturers but can be important in the structure formation of the final MFC.

According to the manufacturer's specifications, YP represents a chemically modified linear LDPE (LLDPE), without pointing out the type or the amount of the modifier. Figure 1 shows a comparison between the FT-IR spectra in transmission mode of the matrix HDPE and the YP compatibilizer. The two spectra are characteristic for polyethylene and display peaks for more than three consecutive $CH_2$ groups (at 1465 and 720−730 cm$^{-1}$), single terminal $-CH_3$ groups (1376 cm$^{-1}$), two $CH_3$ groups in gem-position (1368−1353 cm$^{-1}$) and for trisubstituted CH− groups around 1300 cm$^{-1}$. The formation of a doublet at 720,730 cm$^{-1}$ found in YP is typical of LLDPE polymers.[28,29] The main difference between the spectra of HDPE and YP is the presence in the latter of a clear band at 1791 cm$^{-1}$ for the symmetric stretching vibration of anhydride C═O group ($\nu_{C=O}^{sym}$), the asymmetric vibration ($\nu_{C=O}^{assm}$) being also detectable at 1867 cm$^{-1}$. YP contains also a weak band at 912 cm$^{-1}$ attributed to the ring stretching vibrations of the five-membered saturated anhydride.[30] So it may be concluded that YP contains small amounts of grafted maleic anhydride (MAH). On the basis of the FTIR study of Yang et al.[30] on polyehylene model samples containing various amounts of grafted MAH (0.5−35 wt %) and having in mind the $\nu_{C=O}^{sym}/\nu_{C=O}^{assm}$ intensity ratio in YP in Figure 1a, the MAH content of the YP material was evaluated between 0.5 and 5 wt %. The FTIR studies of Mehrabzadeh et al.[31−33] permitted a more rigorous evaluation of the MAH content. On the basis of the model samples of PE containing 1−5 wt % MAH[33] and by measuring the ratio between the intensities of the MAH band at

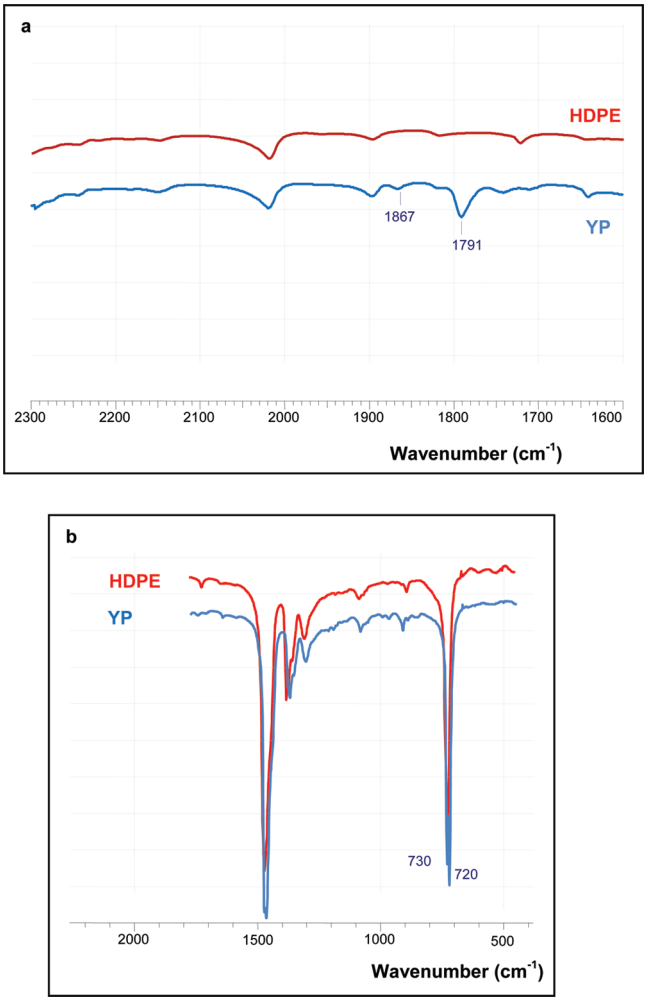


**Figure 1.** FT-IR spectra (transmission mode) of HDPE and YP in the 2300−1600 cm-1 and 1600−500 cm$^{-1}$ ranges .Samples represent ca. 50 $\mu$m thick films obtained by compression molding at 160 °C.

1791 $cm^{-1}$ and the PE band at 720 $cm^{-1}$in Figure 1, it was established that the MAH amount of YP is between 0.5 and 1.0 wt %.

**Sample Preparation.** Granulates of PA12 (dried at 90−100 °C for 6 h), HDPE, and YP (used as received) were premixed in the following proportions: HDPE/PA12/YP = 90/10/0; 80/20/0; 77.5/20/2.5; 75/20/5, 70/20/10; 65/30/5 (wt %). Each mixture was introduced into a laboratory modular Leistritz LSM 30.34 intermeshing corotating twin-screw extruder. The resulting strand was cold-drawn first at 90−95 °C and then at room temperature by passing it through three subsequent haul-off units, whereby the extrudate diameters decreased from 2 mm (at the extruder die) to *ca.* 0.6−0.9 mm at the end of the extruder line. At the exit of the last haul-off device the blends are in the form of oriented, continuous cables (OC). After adequate shaping and unidirectional alignment, the OCs were compression molded at 160 °C to get the MFC in the form of "unidirectional ply lamina" (UDP MFC). Standard rectangular laminate plates (60 × 120 mm with a thickness of 1.0−1.5 mm) were obtained and used for structural and morphological characterization.

**Electron Microscopy.** The samples for SEM were collected at the extrusion die and after the first haul-off unit. Samples of the final MFC were also analyzed. The observation of freeze-fractured specimens sputter-coated with gold was made in a Leica S360 electron microscope.

Because of the low diameter of the OCs and their hardness, it turned impossible to prepare fractured samples of good quality for SEM. However, selected samples were observed by TEM using a Zeiss 902A microscope. The observations were done on ultrathin sections (*ca.* 70 nm) cut at about −130 °C with a Leica FC6 ultramicrotome equipped with diamond knife. Before the observation, the sections were stained with $RuO_4$.

**X-ray Scattering Techniques.** All WAXS and SAXS patterns in this study were registered at the soft condensed matter beamline (A2) of HASYLAB, Hamburg, Germany, using synchrotron radiation with a wavelength fixed to 0.15 nm. The sample-to-detector distance for SAXS was set at 2830 mm, the diffraction patterns being registered by means of a MAR CCD 2D detector. For the WAXS measurements the detector was positioned at 90 mm in respect to the sample. The various MFC were studied in transmission mode the exposure time being 10 s for WAXS and 30 s for the SAXS patterns. A sample holder allowing for controlled heating/cooling cycles in the 30−300 °C range was used.

## Results and Discussion

**SEM Investigations: Proofs for Fibrilar Morphology of MFC.** Figure 2 displays SEM images of PA12-containing materials after the extruder die (column 1), after the first haul-off unit (column 2) and of the final MFC UDP (column 3). In Table 2 the average diameters of the PA12 reinforcing phase derived from the SEM pictures are presented. Comparing the micrographs in Figure 2, column 1, it may be concluded that the diameters of the PA12 globular entities decrease with the increase of the compatibilizer concentration—from > 3000 nm in the 80/20/0 blend to ca. 2500 nm in the compatibilized 70/20/10 blend.

Another observation is that increasing the compatibilizer content results in improved adhesion at the HDPE/PA12 interface. In the blends without (Figure.2, 1a, 2a) or with less compatibilizer (sample 5a) it seems that the PA12 entities are disentangled from the matrix indicating adhesive failure during the cryogenic fracture. Samples 3a, 4a, and 6a, which contain 5−10% Yparex, show cohesive fracture in the PA12 reinforcing elements without separation of the latter from the matrix.

As expected, as the materials pass through the first haul-off unit, the diameters of the PA12 entities decrease significantly in all compositions (Figure 2, samples 1b−6b, and Table 2). This is an indirect indication that an additional stretching of the PA12 phase was induced at this stage.

The fibrils' orientation and morphology could be observed in the final MFC after fracturing the specimens in a direction parallel to the fibrils (Figure 2, samples 1c−6c, and Table 2). The fibril thicknesses depend on the YP and PA content and vary in a broad range between 500 and 1250 nm. The finest fibrils are observed in the 90/10/0 sample and in the 70/20/10 MFC, the latter containing the biggest amount of compatibilizer (images 1c and 3c). The micrographs of the YP containing samples show clearly the above-mentioned improved adhesion in the presence of compatibilizer. The fibrils look like being "cemented" into the HDPE matrix, which is not the case in images (images 1c, 2c) where the fibrils are smoother and are, apparently, separated from the matrix.

The influence of compatibilizer on the PA12 composite morphology is further revealed in Figure 3. All images were obtained after selective extraction of the HDPE matrix with hot toluene for 5 h. The PA12 reinforcing fibrils are with average diameters of 525 nm (no compatibilization, image 1a in Figure 3, Table 2) and 450 nm for the sample with the largest concentration of compatibilizer (image 2a). Interestingly, the selective dissolution seems to remove the same amount of matrix material (ca. 18%) from the HDPE/PA12 composites with and without compatibilizer. This was not the case with the HDPE/PA6MFC where the 70/20/10 sample showed the same fibril thickness and aspect ratios (AR) before and after dissolution.[17] To explain this difference, one should consider the studies on the chemical reaction between polyethylene/MAH copolymers and amine groups from polyamides[34,35] suggesting chain scission and formation of imide linkages, thus creating chemical bonds at the polyolefin/polyamide interface. Therefore, since PA12 contains only the half of the NH groups of PA6, the number of the effective imide linkages will be reduced causing weaker attachment at the interface. In the case of YP-compatibilized HDPE/PA12 blends, chemical bonds can only be realized between PA12 and the LLDPE-*co*-MAH of YP, as the matrix HDPE does not have MAH functionality (Table 1).

The images after selective dissolution of samples obtained at the extruder die (Figure 3, images 1b and 3b) display dendrite structures containing oriented stem entities of considerable thickness: from 1− 2 (compatibilized) to 3−4 $\mu$m (noncompatibilized) implying certain orientation even right after the extruder die.

Figure 4 shows the TEM micrograph of the 77.5/20/2.5 oriented cable. The PA12 reinforcing phase is well distributed within the HDPE matrix. The PA12 fibrils' diameters vary in the 100−400 nm range, i.e. in the oriented precursor blends they are significantly thinner than those in the final MFC (ca. 750 nm).

A possible explanation of this fact is the appearance of a TCL layer of HDPE upon the PA12 fibril during the compression molding stage when the finale MFC is obtained. It can be supposed that the reinforcing fibrils in the MFC most probably contain a core of PA12 and a shell of transcrystalline HDPE. Thus, on the basis of the electron microscopy experiments, the following model can be suggested visualizing the structural changes during the MFC preparation (Figure 5).

According to the model proposed, right after the extruder die, the PA12 globules are embedded into an isotropic HDPE major phase. During the cold drawing stage, i.e., in the oriented precursor cables, both HDPE and PA12 are fibrillated. During the compression molding at 160 °C, the HDPE

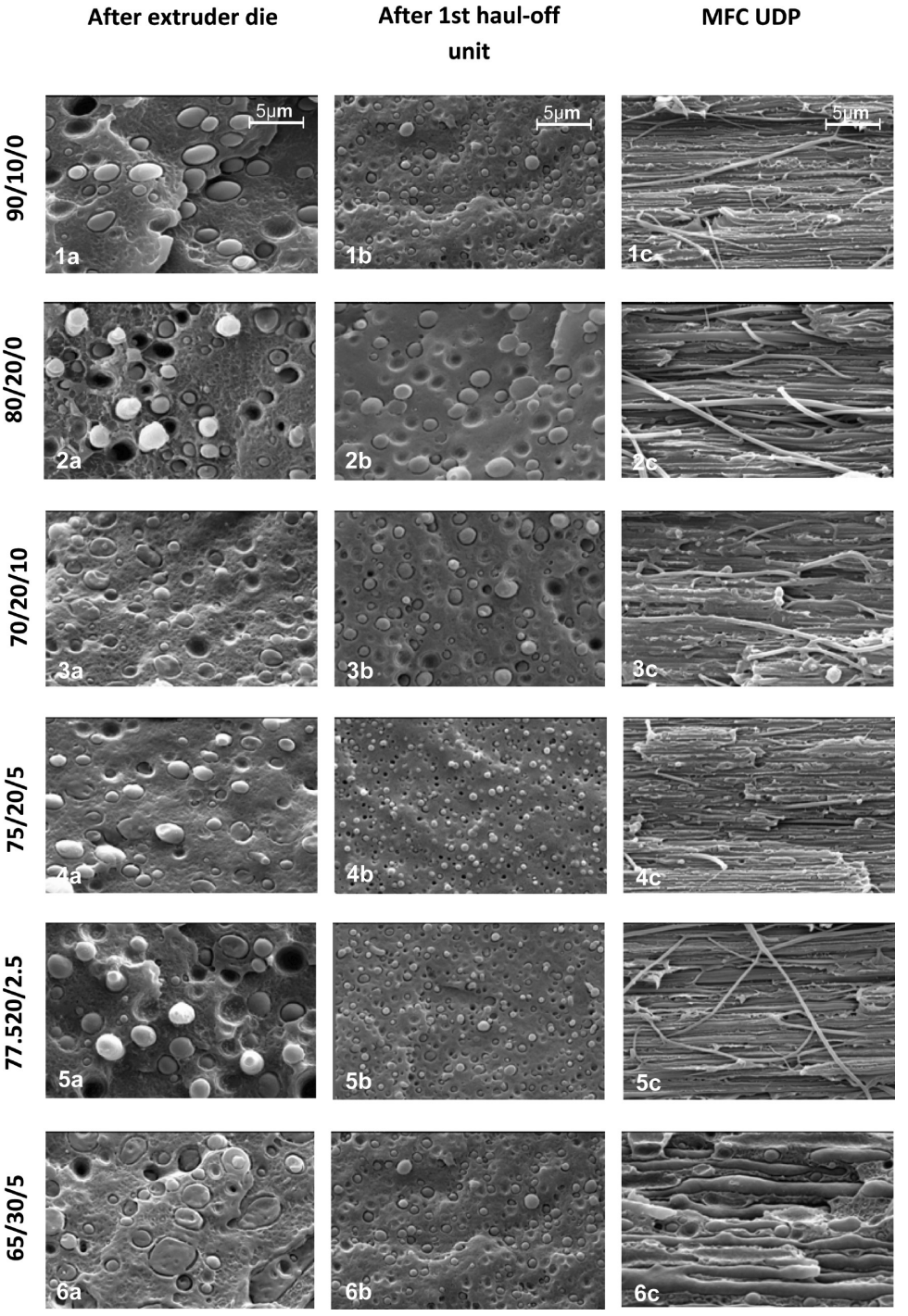


**Figure 2.** SEM images of cryogenic fractured surfaces of various HDPE/PA12/YP materials (compositions given in wt %) during the stages of the MFCs preparation: nonoriented blend after the extruder die (1a−6a); slightly oriented blends after the first haul-off unit (1b−6b); MFC UDP, fractured in the direction of the fiber (1c−6c).

fibrils melt and upon the subsequent cooling and crystallization of the matrix, the PA12 fibrils are coated with a TCL of HDPE material.

The model in Figure 5 suggests that each fibril is produced by elongation of one single polyamide globule. As shown by Fakirov et al,[36] the fibril formation in MFC precursors produced by drawing of PP/PET blends with compositions close to 50//50 wt % should be attributed to coalescence of PET globules and not to their deformation. In our case, however, the PA12 content in the MFC studied is lower, in the 10−30 wt % range, which makes coalescence significantly less probable, especially in the samples with 10 and 20% of PA12. Moreover, one has to keep in mind that the cold drawing in the MFC preparation was performed at 90−95 °C, *i.e.*, far below the melting point of PA12 (Table 1). At such low temperatures the coalescence process will be additionally hindered because of the poor diffusion conditions as compared to the case of molten polymers.[37]

None of the micrographs of MFC permits to measure directly the fibril length. Indirectly, the average lengths and aspect ratios of the reinforcing PA12 fibrils can be estimated on the basis of the model in Figure 5. Supposing that the contribution of coalescence is negligible and that spherical PA12 entities are transformed into the final fibrils without

**Table 2. Dimensions of the PA12 Reinforcing Phase in Various HDPE/PA12/YP Materials As Revealed by the SEM Measurements[a]**

| composition, HDPE/PA12/YP wt % | diameters of PA12 nodules at ED, nm | dimensions of the PA12 fibrils after the 1st haul-off unit, nm | | | dimensions of the PA12 fibrils in UDP MFC, nm | | |
|---|---|---|---|---|---|---|---|
| | | av diameter | avlength | av aspect ratio | av diameter | av length | av aspect ratio |
| 90/10/0 | 2500 | 1500 | 4630 | 3.1 | 500 | 41 700 | 83 |
| 80/20/0 | 3125 | 2200 | 4200 | 1.9 | 625 (525) | 52 100 (52100) | 83 (99) |
| 70/20/10 | 2500 | 1500 | 4630 | 3.1 | 560 (450) | 33 216 (33216) | 59 (74) |
| 75/20/5 | 1875 | 1000 | 4395 | 4.4 | 625 | 11 250 | 18 |
| 77.5/20/2.5 | 2500 | 1000 | 10 417 | 10.4 | 750 | 18 518 | 25 |
| 65/30/5 | 5000 | 1500 | 37 037 | 24.7 | 1250 (900) | 53 333 (53333) | 43 59 |

[a] The values in brackets are observed after selective extraction of the HDPE matrix. Note: ED = extruder die; UDP = unidirectional ply lamina.

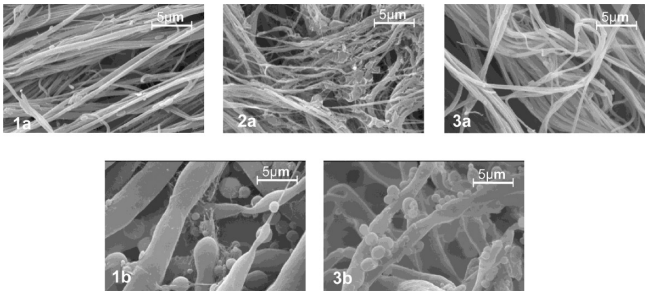


**Figure 3.** SEM images of various HDPE/PA12/YP samples after selective extraction of the matrix (a, final MFCs; b, nonoriented blends after the die exit) with the following compositions (wt %): 1, 80/20/0; 2, 70/20/10; 3,- 65/30/5.

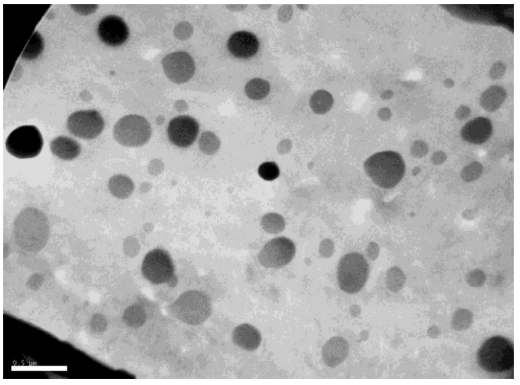

**Figure 4.** TEM image of 77.5/20/2.5 HDPE/PA12/YP oriented precursor obtained after the second haul-off unit. The white bar corresponds to 500 nm.

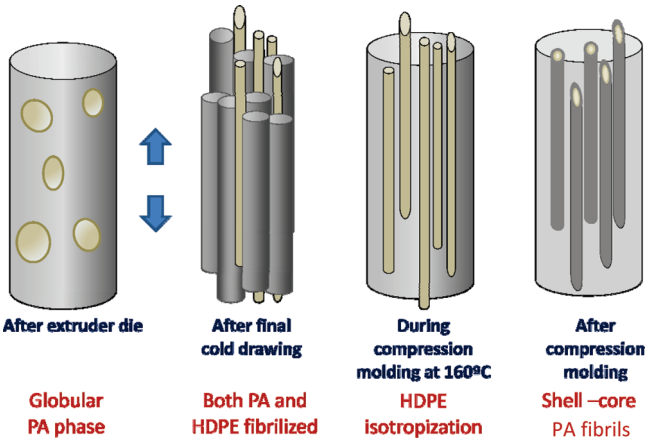


**Figure 5.** Simplified model of the structural changes occurring at different stages of the MFC preparation.

the formation of voids (i.e., the volume of the PA12 spheres at the extruder die and of the MFC fibril are the same), it is possible to estimate the average length, $L$, of the fibrils and thereafter the aspect ratio, AR (Table 2). Thus, in noncompatibilized PA12-reinforced MFC the calculated lengths of the reinforcing fibrils is in the range between 42 and 52 $\mu$m and with YP (20% PA12)—from 11 to ca. 33 $\mu$m. It can be seen also that the two noncompatibilized samples showed the highest maximum AR values ($>80$), and that the latter fluctuated with the YP content. In fact, having in mind the decrease of the fibrils' diameters after selective extraction, the real AR values should be even larger. A possible way to assess the real AR is to obtain an estimate of the TCL thickness.

**SAXS Studies of HDPE/PA12/YP MFC.** Figure 6 shows the SAXS patterns of three representative HDPE/PA12/YP UDP MFC compositions (after corrections for the empty chamber scattering and for the intensity of the primary beam): without compatibilizer, (1) 80/20/0; with compatibilizer, (2) 70/20/10 and (3) 75/20/5 at different temperatures. It can be seen that at 30 °C the three MFC contain both isotropic scatterers, producing the circular reflection with a long spacings ($L_B$) of approximately 220 Å, and oriented ones giving rise to the two point-like reflections oriented along the horizontal axis of fibril orientation and with very similar $L_B$ values (Table 3). The latter cannot belong to the reinforcing oriented PA12 whose typical $L_B$ is in the range 100−110 Å.[26,27] Therefore, it can only be attributed to the scattering of HDPE (or, in compatibilized systems, of LLDPE) oriented material crystallized upon the PA12 fibrils. The oriented reflections of PA12 can be visualized only after the matrix melting at 160 °C (Figure 6, second column). While the $L_B$ of the sample without compatibilizer (pattern 1b) is consistent with the neat PA12, that of the sample containing 5 and 10% compatibilizer shows scattering with larger $L_B$ of 120 and 130 Å, respectively. Most probably, these oriented reflections in patterns 2b and 3b at 160 °C originate from LLDPE/MAH-*co*-PA12 block copolymer obtained through the reaction of the YP and PA12, being still crystalline and oriented at 160 °C. The SAXS patterns obtained at 30 and 160 °C give a strong evidence of the presence of oriented PE in the final MFC thus proving the shell−core morphology of the reinforcing fibers, comprising a core of oriented PA12 with a shell of oriented, transcrystalline PE (HDPE or LLDPE).

It is interesting to compare the SAXS patterns of the three starting MFC at 30 °C (Figure 6, column 1) and those obtained after their recrystallization carried out in the beam (30 °C after 160 °C), (column 3). They are not identical. It can be seen that upon recrystallization meridional point-like reflections (*i.e.*, perpendicular to the axis of fiber alignment) also appear, better seen in the noncompatibilized sample.

**Table 3. Bragg's Long Spacing Values of HDPE/PA12/YP UDP MFC at 30°C and after Matrix Recrystallization (at 30 °C after 160 °C)[a]**

| | SAXS at 30 °C | | | | SAXS at 30° after 160 °C | | | |
|---|---|---|---|---|---|---|---|---|
| | isotropic scattering | oriented scattering | | | isotropic scattering | oriented scattering | | |
| HDPE/PA12/YP UDP MFC composition wt % | $L_B$ HDPE, Å | $L_B^{Eq}$* PE, Å | $L_B^{Mer}$* PE, Å | $L_B^{Eq}$PA12, Å | $L_B$ HDPE, Å | $L_B^{Eq}$* PE, Å | $L_B^{Mer}$* PE, Å | $L_B^{Eq}$PA12, Å |
| 90/10/0 | 220 | 229 | 251 | 91 | 229 | 235 | 251 | 108 |
| 80/20/0 | 216 | 235 | 256 | 101 | 218 | 253 | 268 | 112 |
| 77.5/20/2.5 | 215 | 220 | | 100 | 218 | 248 | 255 | 120 |
| 75/20/5 | 213 | 229 | | 97 | 244 | 242 | 244 | 118 |
| 70/20/10 | 208 | 233 | | 96 | 225 | 215 | 229 | 124 |
| 65/30/5 | 218 | 229 | | 99 | 218 | 250 | 265 | 118 |

[a] Note: $L_B^{Eq}$* = long spacing of the PE lamellae oriented along the equator; $L_B^{Mer}$* = long spacing of the PE lamellae oriented along the meridian. The fiber direction coincides with the equator. Oriented PE includes fractions of the matrix HDPE or LLDPE of YP.

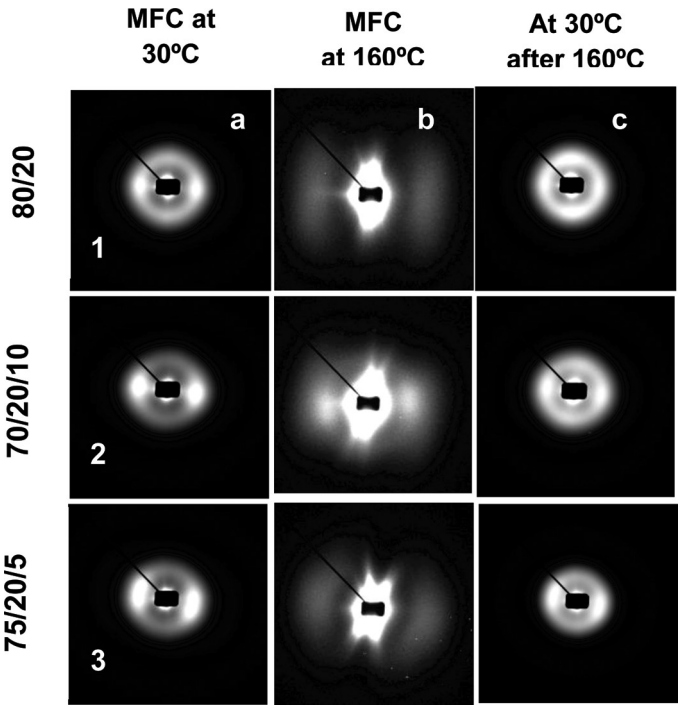


**Figure 6.** 2D SAXS images of different HDPE/PA12/YP UDP MFC: column a, as prepared, at 30 °C; column b, at 160 °C, in-beam heating; column c, at 30 °C after heating to 160 °C (recrystallization).

This tendency can be quantified in the azimuthal scans of SAXS patterns before and after recrystallization, as a function of the YP content of the sample (Figure 7).

Figure 7a shows that the initial composites without compatibilizer (1 and 2), display both meridional and equatorial scattering, while those with compatibilizer (3 and 4) scatter in equatorial direction only. After selective melting of the matrix at 160 °C and its subsequent recrystallization (Figure 7b), all patterns show bimodal distribution of the oriented scattered intensity. This means that after recrystallization in all samples the transcrystalline layer contains PE lamellae (periodicities) oriented along and perpendicular to the fiber axis.

To quantify better the contributions of the isotropic and oriented scattering and to relate them with the existing phases, the POLAR 2.7.1 X-ray software[38] was used. A built-in procedure allowed the separation of the total scattered intensity of the 2D SAXS patterns into two contributions—isotropic and oriented. The oriented component is calculated by subtracting the azimuthally independent component from the total SAXS intensity.[39,40] This procedure is visualized in Figure 8 for two samples: 80/20/0 and 70/20/10 UDP MFC. Images a and d represent the initial SAXS patterns; b and e are of the computed isotropic intensities; c and f represent the resulting oriented scattering. Patterns c and f reveal the presence of oriented PA12 reflections and confirm the data from the azimuthal scans about the existence of PE lamellae with various orientations. The 3D images in Figure 9 display better the contribution of the PA12 phase along the equator (the vertical arrows) and also two types of oriented PE scattering—equatorial and meridional, the latter being indicated with horizontal arrows. The meridional PE scattering clearly exists in patterns c and d obtained after matrix recryslaization. It exists also in the noncompatibilized MFC before recrystallization (Figure 9a), but not in the compatibilized one (Figure 9b). In the case of HDPE/PA6 UDP MFC we observed such meridional behavior of the oriented PE only after recrystallization and only in the samples without compatibilizer.[17]

The isotropic part of the 2D SAXS patterns was sectioned in the range of 0−180° and the Bragg's long spacing $L_B$ ascribed to isotropic HDPE was determined. Two sections of the oriented patterns were made: (i) along the equator (−45° − +45°) giving rise to $L_B^{Eq}$* and $L_B^{Eq}$ and (ii) along the

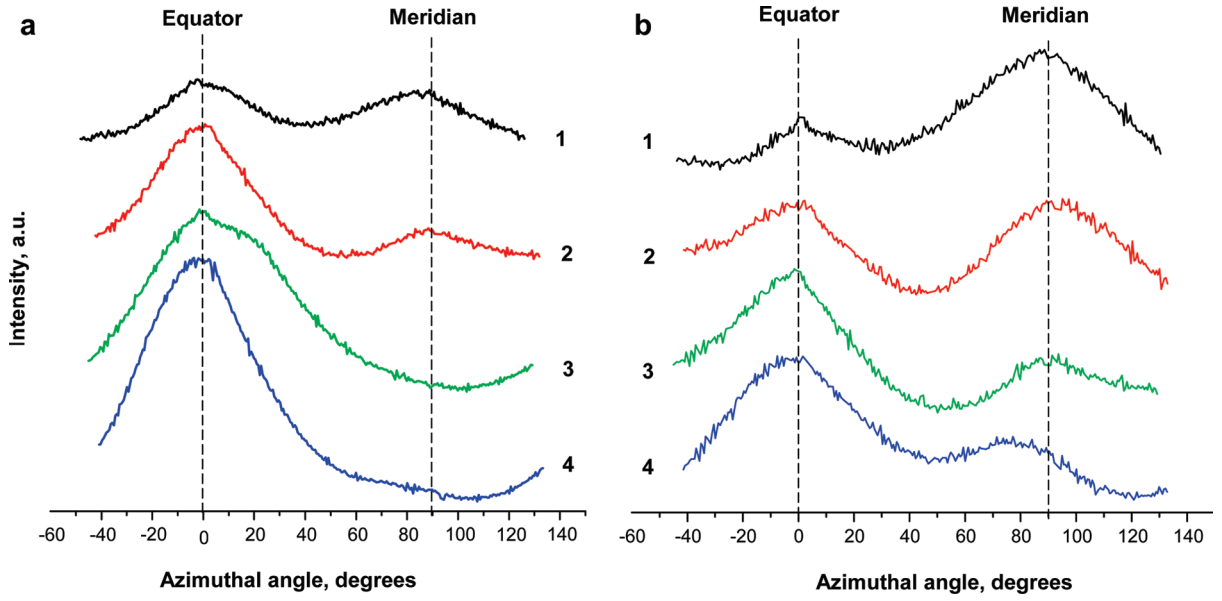


**Figure 7.** Azimuthal distribution of the scattered intensity in the 2D SAXS images of HDPE/PA12/YP UDP MFCs obtained at: 30 °C (a) and at 30 °C after heating to 160 °C (recrystallization) (b). The compositions are as follows: 1, 90/10/0; 2, 80/20/0; 3, 75/20/5; 4, 70/20/10.

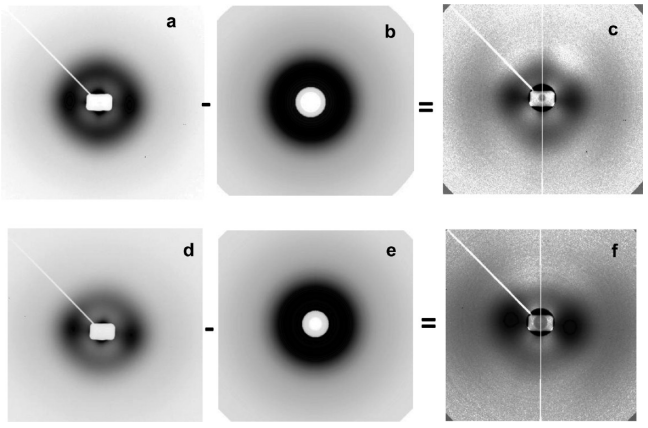


**Figure 8.** Separation of the oriented and isotropic scattering with the SAXS pattern of the 80/20/0 UDP MFC (a−c) and 70/20/10 UDP MFC d-f): (a and d) initial 2D patterns; (b and e) computer generated patterns of the isotropic scattering; (c and f) intensity pattern of the oriented scatterers obtained by subtraction of the central images from the left ones. The fiber axis is horizontal.

meridian (45° − 135°) for $L_B^{Mer}$* (Table 3). It can be seen that the oriented PE lamellae have bigger periodicities than the isotropic ones. Also, in the as-prepared MFC the $L_B^{Eq}$* periodicity of PE is always present, fluctuating around 230 Å, independently of the YP content, whereas $L_B^{Mer}$* > 250 Å only appear in the noncompatibilized MFC. Changes toward increasing of both PE periodicities occur upon matrix recrystallization. Generally, the PE lamellae along the meridian have bigger long spacings as compared to those of the PE crystallized along the fiber direction. The PA12 long spacings $L_B^{Eq}$ are between 90 and 100 Å in the MFC prior to recrystallization, which is in good agreement with the values of the neat oriented PA12.[27] After recrystallization a significant growth of $L_B^{Eq}$ is registered—between 11 Å in the 80/20/0 MFC and 28 Å in the YP-reach 70/20/10 MFC. It seems that compatibilization results in changes in both PE and PA12 phases, which in the SAXS patterns become clearer after matrix recrystallization.

**WAXS Studies of HDPE/PA12/YP MFC.** To obtain a different inside on the structural changes in PA12 and PE phases in compatibilized and noncompatibilized MFC, WAXS studies were performed. Figure 10 displays 2D WAXS patterns of HDPE/PA12/YP MFC with unidirectional alignment of the reinforcing fibrils, with and without compatibilizer at 30 °C, 160 and 30 °C after matrix recrystallization at 160 °C. Judging from the meridional point-like reflections (fiber axis is horizontal), ascribed to the γ-PA12 0k0 planes that appear at the three temperatures, it can be concluded that under these conditions there exist significant amounts of γ PA12 polymorph. The two Debye rings in the patterns at 30 °C should be related to the presence of isotropic HDPE, whose (110) plane (the internal ring) and (200) plane (the external one), are superimposed with the equatorial PA12 oriented reflections characterizing its (001) and (200) planes.

To study the crystalline structure of the PA12 core of the fibrils, the 2D WAXS patterns at 160 °C were sectioned and the respective 1D profiles deconvoluted by commercial peak-fitting software. Figure 11 exemplifies the fit of the 70/20/10 UDPE MFC at 160 °C. There is overlapping of many reflections in the 2θ range studied, but with the help of the results obtained from the detailed investigation on neat PA12[26,27] their identification was possible in the MFC. The deconvoluted reflections of the two PA12 polymorphs in the order of increasing 2θ are as follows: γ(020); α(100); γ(040); α(200); γ(001); γ(200); α(002). As seen from Figure 11, there exist considerable amounts of α-PA12 polymorph (the shaded peaks) in the 70/20/10 MFC. Table 4 summarizes the polymorph composition of all HDPE/PA12/YP UDP MFC at 160 °C obtained analogously.

Table 4 shows that the crystallinity index of the PA12 fibrils at 160 °C varies between 35 and 43%, comprising various proportions of α and γ-PA12. The γ/α ratio is the biggest (γ/α = 2.1) in the 90/10/0 composition. Within the samples containing 20% PA12, the γ polymorph is predominant in the 80/20/0 system (γ/α = 1.48), while the 70/20/10 composite, which contains the biggest YP concentration, i.e., the largest amounts of LLDPE chemically attached to PA12, is richer in the α PA12 form (γ/α = 0.65).

To study the WAXS patterns of the as-prepared MFC at 30 °C trying to evaluate the TCL, the total scattered intensity was separated into two contributions—oriented and

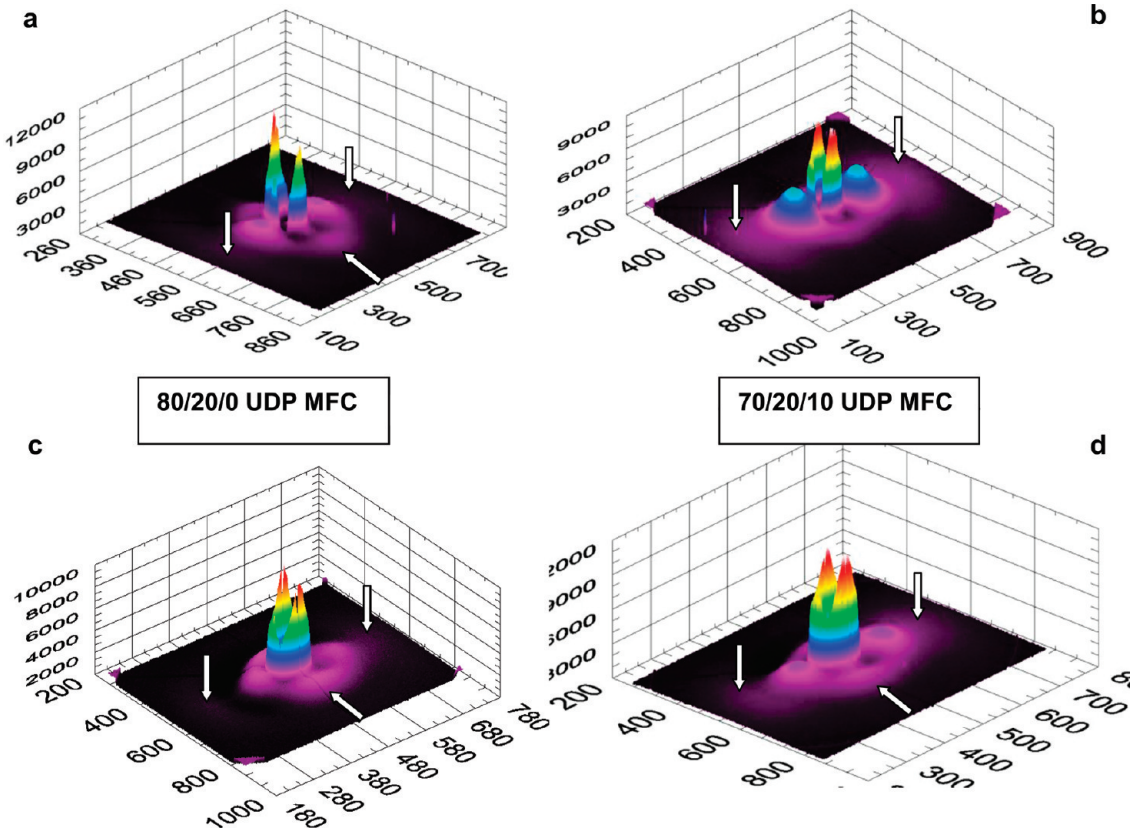


**Figure 9.** 3D projections of the oriented SAXS scattering of two HDPE/PA12/YP composites. Initial composites at 30 °C: (a) 80/20/10 and (b) 70/20/10. The same composites after selective matrix recrystallization (in beam heating), images c and d, respectively. For more details see the text.

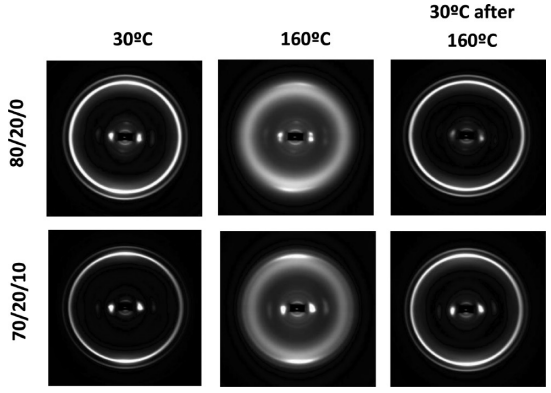


**Figure 10.** 2D WAXS patterns of HDPE/PA12/YP UDP MFC taken at various temperatures. The fiber axis is horizontal.

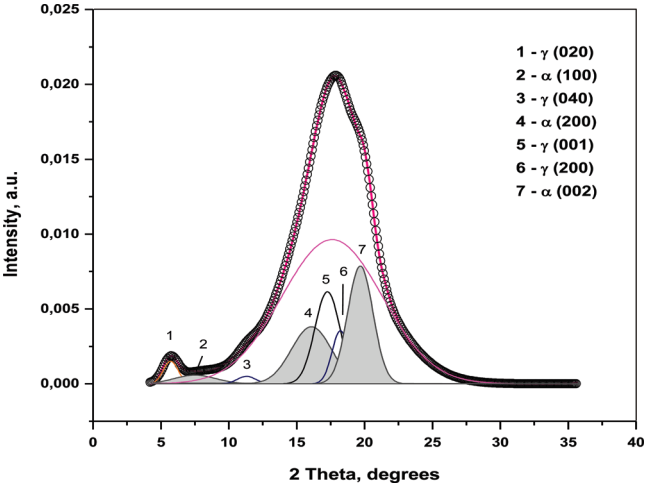


**Figure 11.** Peak fitting of 1D WAXS curve of the 70/20/10 UDP MFC at 160 °C. The shaded peaks belong to α-PA12. The broad peak centered at $2\theta = 18°$ originates from the diffuse scattering of the amorphous material.

isotropic as in the SAXS data handling, using the same software and procedures. The final results of this subtraction procedure are displayed in Figure 12, where the oriented WAXS scattering of two typical patterns of MFC without (a) and with compatibilization (b) are presented. One can observe the anisotropy of the (110) and (200) PE reflections, as well as some of the oriented equatorial and meridional reflections of the PA12 phase: 1, α(100); 2, γ(020); 3, γ(040); 4, α(200). It should be noted that the chain direction of PA12 and that of the oriented PE fraction coincide in both compatibilized and noncompatibilized HDPE/PA12/YP MFC. This is true not only in the as-prepared MFC at 30 °C (Figure 12) but also for MFC samples after recrystallized at 160 °C

Figure 13 shows the peak-fitted 1D WAXS profiles of a compatibiized MFC sample (HDPE/PA12/YP = 70/20/10). As seen from the deconvolution of the oriented scattering

**Table 4. PA12 Polymorph Content in HDPE/PA12/YP MFC at 160 °C[a]**

| composition HDPE/PA12/YP ,wt % | vol. fract. of PA12, % | α form, % | γ form, % | γ/α | CI, % |
|---|---|---|---|---|---|
| 90/10/0 | 0.094 | 11.3 | 23.8 | 2.10 | 35.1 |
| 80/20/0 | 0.189 | 16.9 | 25.0 | 1.48 | 41.9 |
| 70/20/10 | 0.188 | 23.7 | 15.4 | 0.65 | 39.1 |
| 75/20/5 | 0.189 | 19.6 | 23.7 | 1.20 | 43.3 |
| 77.5/20/2.5 | 0.189 | 20.0 | 21.2 | 1.06 | 41.2 |
| 65/30/5 | 0.285 | 20.5 | 20.7 | 1.01 | 41.2 |

[a] Notes: CI = crystallinity index. CI = αCI + γCI; αCI = α(100) + α(200) + α(002); γCI = γ(020) + γ(040) + γ(001) + γ(100).

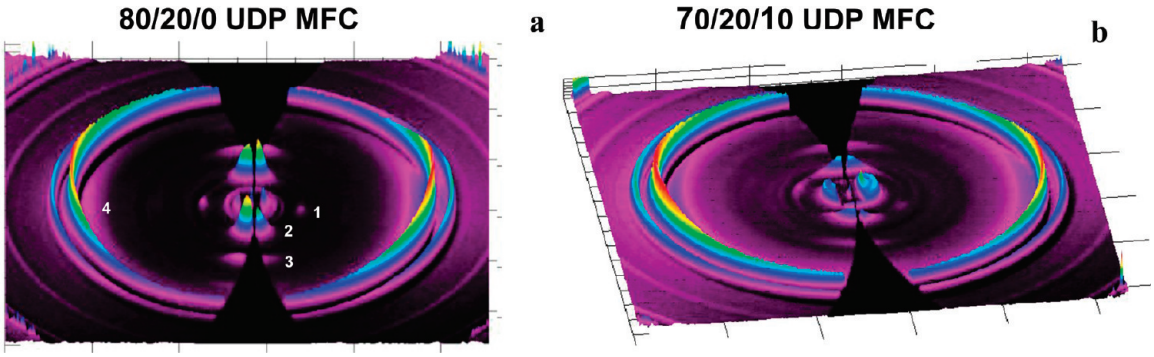


**Figure 12.** Frazer corrected 3D WAXS patterns at 30 °C after subtraction of the isotropic component of (a) 80/20/0 MFC UDP; (b) 70/20/10 MFC UDP. The numbers indicate the following PA12 crystalline planes: 1, α(100); 2, γ(020); 3, γ(040); 4, α(200). The fiber axis is vertical.

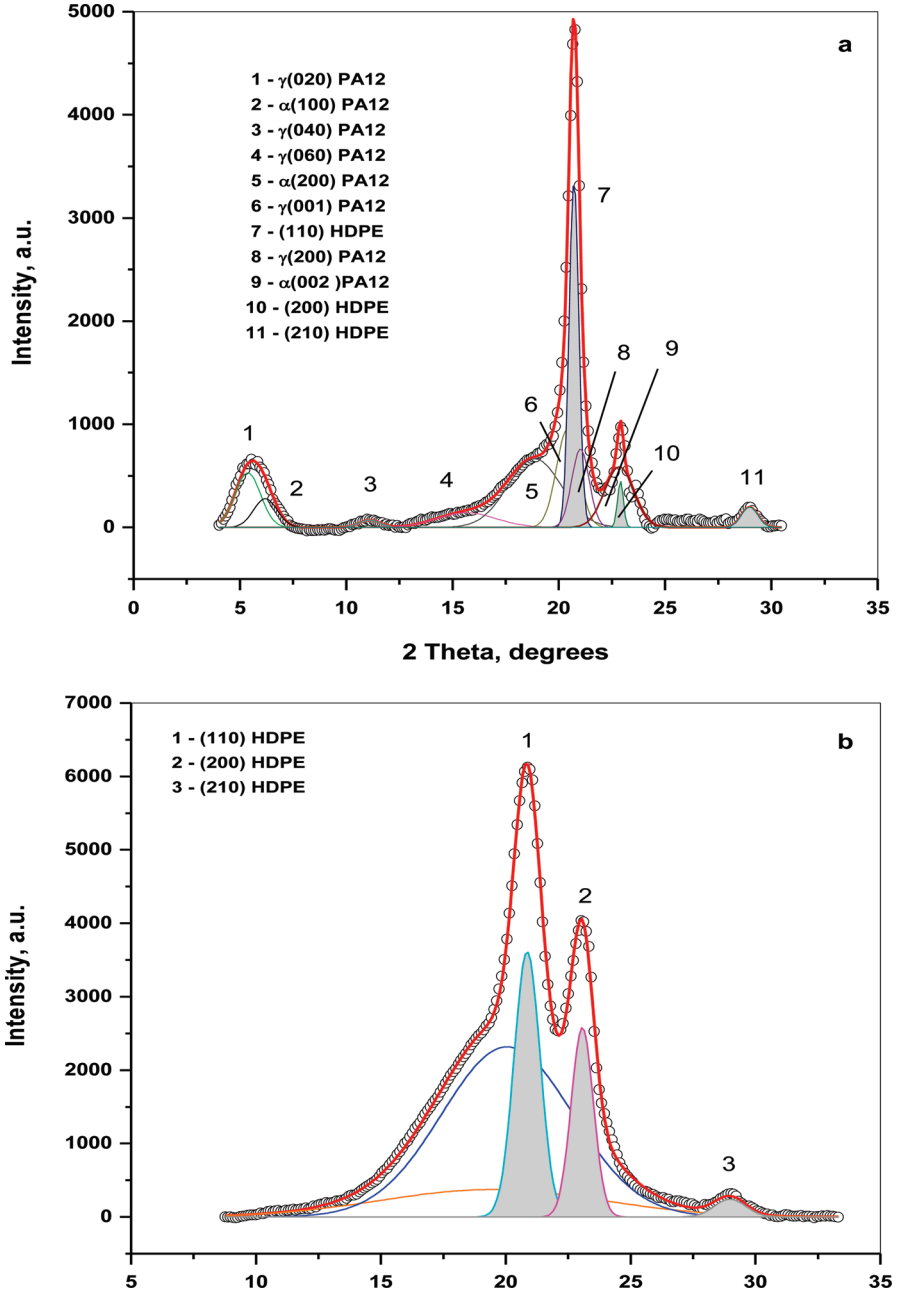


**Figure 13.** 1D WAXS profiles of the 70/20/10 HDPE/PA12/YP UDP MFC depicting the peak-fitting of the oriented WAXS scattering (a) and of the isotropic WAXS scattering (b).

**Table 5. Results from the Deconvolution of the Oriented Part of 2D WAXS Patterns of HDPE/PA12/YP UDP MFC[a]**

| composition HDPE/PA12/YP, wt % | α-PA12, % | γ-PA12, % | PA12 total, % | HDPE (oriented), % | *f* | [HDPE]* (oriented), wt % |
|---|---|---|---|---|---|---|
| 90/10/0 | 21.7 | 43.6 | 65.3 | 34.7 | 1.883 | 5.31 |
| 80/20/0 | 42.2 | 31.6 | 73.8 | 26.2 | 2.817 | 7.10 |
| 70/20/10 | 28.9 | 37.1 | 66.0 | 34.0 | 1.942 | 10.30 |
| 75/20/5 | 13.2 | 54.2 | 67.4 | 32.6 | 2.066 | 9.68 |
| 77.5/20/2.5 | 19.9 | 49.0 | 68.9 | 31.1 | 2.217 | 9.02 |
| 65/30/5 | 23.8 | 47.3 | 71.1 | 28.9 | 2.463 | 12.19 |

[a] Notes: The coefficient *f* is the relationship between the PA12 and HDPE fractions of the oriented scattering; The [HDPE]* (oriented) represents the oriented part of the PE material (matrix HDPE and/or LLDPE from YP) if the PA12 is assumed to be 100% fibrilar.

(Figure 13a), the main reflections of the PE (shaded peaks) overlap with those of the α-PA12 (peaks 5 and 9) and γ-PA12 polymorphs (peaks 6 and 8). Altogether, the following reflexes were identified (given in increasing $2\theta$ order): γPA12-(020); αPA12(100); γPA12(040); γPA12(060); αPA12(200); γPA12(001); PE(110); γPA12(200); αPA12(002); PE(200); PE(210). The peak-fitting of the isotropic part (Figure 13b) displayed crystalline reflections only of the HDPE matrix, indexed as (110), (200), and (210), along with the amorphous halos of PA12 and HDPE.

The WAXS patterns of all MFC were treated analogously. The data in Table 5 show that in all compositions investigated there exist a part of PE that crystallizes orientated along the PA12 fibrils. The percentage of this part varies between 26% and 35% of the total oriented scattering and depends on the PA12 concentration—it is the highest in the sample with 10% PA12 and the lowest in the 65/30/5 composition. Assuming that PA12 phase is 100% fibrilar, the fraction of the oriented polyethylene [PE]* in the respective MFC can be calculated. It can be seen that the [PE]* increases as the PA12 content grows from 10 to 30%. Another observation is that the YP concentration has also some influence—the bigger the YP content, the larger is the [PE]* amount that crystallizes oriented along the PA12 fibrils.

**Estimation of the TCL Thickness from WAXS and SEM Data.** The combination of data from SEM and WAXS analyses allowed the approximate estimation of the TCL thickness. According to the model in Figure 5, the reinforcing fibril in the final MFC is cylindrical comprising a core of oriented PA12 and a coaxial shell of oriented HDPE (Figure 14A). It can be seen that:

$$V_{\mathrm{PA12}} = \pi {R_1}^2 L \tag{1}$$

and

$$V_{\mathrm{TCL}} = \pi L({R_2}^2 - {R_1}^2) \tag{2}$$

where $R_2$ is the outer (i.*e*, visible by SEM) radius of the fibril, and $R_1$ is the radius of the PA12 core. The $V_{\mathrm{PA12}}$ and $V_{TCL}$ are the volumes of the PA12 and transcrystalline oriented HDPE. Each of the two volumes will be proportional to the respective part of the oriented WAXS intensity, i.e.,

$$I_s^{\mathrm{PA12}} \sim V_{\mathrm{PA12}}\rho_{el}^{\mathrm{PA12}} \quad \text{and} \quad I_s^{\mathrm{PA12}} \sim V_{\mathrm{PA12}}\rho_{el}^{\mathrm{PA12}} \tag{3}$$

Here, $\rho_{el}$ represents the volume average electron density of either PA12 or HDPE calculated in the following way:[41]

$$\rho_{el} = N_{\mathrm{A}}\frac{Z_M}{M_M}\rho_m \ [\text{electron units/nm}^3] \tag{4}$$

$N_A$ being the Avogadro's number, $Z_M$ the number of electrons per repeat unit, $M_M$ the molecular weight of the repeat unit, and $\rho_m$ the average mass density. The average electron densities of HDPE and PA12 were found to be 347 and 339 eu/nm$^3$, respectively.

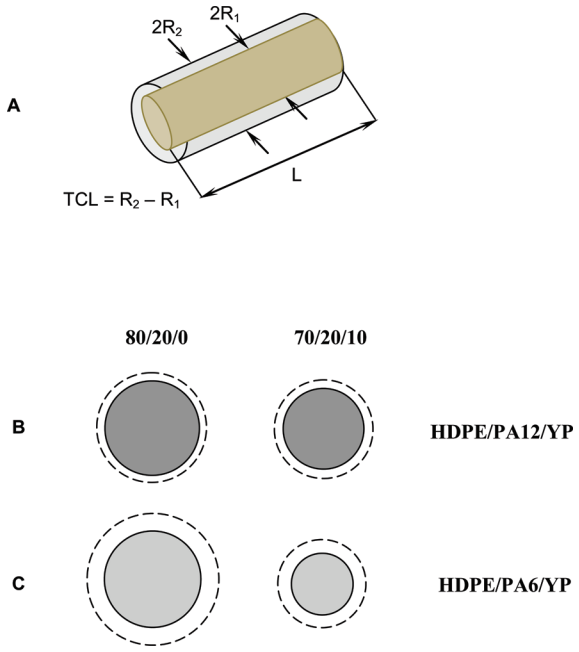


**Figure 14.** Idealized model of the PA12 fibril: A, representation of core, shell and TCL thicknesses; B and C, to-scale representations of the cross sections of the PA12 and PA6 reinforcing fibril in two HDPE/PA/YP MFCs—80/20/0 and 70/20/10. The solid circles represent the polyamide fibers, and the dashed circles represent the transcrystalline HDPE layer. For more details see the text.

After dividing eq 1 by eq 2 and rearrangement, the following expression is obtained

$$2R_1 = 2R_2\sqrt{\frac{f}{k+f}} \tag{5}$$

wherein *f* is the relationship between the PA12 and HDPE fractions of the oriented scattering (Table 5) and $k = \rho_{el}^{\mathrm{PA12}}/\rho_{el}^{\mathrm{PE}}$. Using eq 5, the TCL thicknesses in all MFC under investigation were calculated and also the real AR of the PA12 reinforcing fibrils, *i.e*., after elimination of the thickness of the HDPE shell (Table 6). It should be noted that the real AR values almost coincide with those obtained after selective extraction of the HDPE component (Table 2, last column), which is a corroboration of the credibility of the methods for TCL estimation applied.

From Table 6, it can be also seen that the TCL in the HDPE/PA12/YP composites varies in the 43−96 nm range being the finest in the samples without compatibilizer, the same showing also the largest fibril length, *L*. Generally, compatibilization results in an increase of TCL and in a more pronounced decrease of *L*. Figure 14b visualizes the cross

**Table 6. Variation of Some Structural Parameters of the Reinforcing Fibrils in HDPE/PA12/YP MFC As Revealed by SEM and WAXS Studies[a]**

| sample composition, wt % | $2R_2$, nm | $2R_1$, nm | TCL, nm | $L$, $\mu$m | AR | real AR |
|---|---|---|---|---|---|---|
| 90/10/0 | 500 | 406 | 47 | 41.7 | 83 | 102 |
| 80/20/0 | 625 | 539 | 43 | 52.0 | 83 | 97 |
| 70/20/10 | 560 | 456 | 52 | 33.2 | 59 | 73 |
| 75/20/5 | 625 | 515 | 55 | 11.2 | 18 | 22 |
| 77.5/20/2.5 | 750 | 624 | 63 | 18.5 | 25 | 30 |
| 65/30/5 | 1250 | 1058 | 96 | 53.3 | 43 | 50 |
| 80/20/0[b] | 750 | 550 | 100 | 50.8 | 68 | 92 |
| 70/20/10[b] | 500 | 350 | 75 | 4.6 | 9 | 13 |

[a] Key: $2R_2$, fibril diameter visible by SEM; $2R_1$, diameter of the PA12 core calculated by eq 5; thickness of the oriented HDPE shell; visible AR = $L/R_2$; real AR = $L/R_1$. [b] Data for HDPE/PA6/YP MFC.[17]

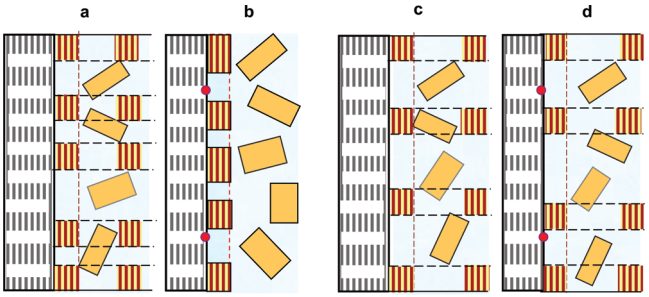


**Figure 15.** Structural models of noncompatibilized (a and c) and compatibilized (b and d) HDPE/PA12/YP UDP MFCs. (a and b) Structure of the as-prepared MFCs. (c and d) Structure after in-beam matrix recrystallization. The red points represent the chemical bonds between the PA12 and Yparex. The vertical short solid lines indicate the chain direction in the lamellae. The dashed lines sketch out the presence of correlation of lamellae parallel and perpendicular to the PA12 fibers.

sections of these fibrils in two selected HDPE/PA12/YP samples without and with compatibilizer. For the 80/20/0 sample $2R_2/2R_1$/TCL = 625/539/43 nm. In the compatibilized sample (70/2010), the core and the total diameters decrease, while the TCL grows with 9 nm and $2R_2/2R_1$/TCL = 560/456/52 nm. The cross sections of the respective HDPE/PA6/YP determined analogously[17] are characterized by larger TCL thicknesses, especially in the noncompatibilized 80/20/0 sample with TCL =100 nm. The addition of 10% of compatibilizer in PA6-reinforced MFC results in a decrease of TCL thickness to 75 nm and in much stronger drop of the AR (Table 6, asterisk marked samples). It will be of some interest to relate the thickness and morphology of the TCL with the mechanical properties of the MFC materials with either PA6 or PA12 fibril reinforcement. These studies are now in progress and will be communicated separately.

**Structural Models of HDPE/PA12/YP MFC.** On the basis of the microscopy and X-ray studies in this work we suggest the following models (Figure 15) to describe the nanostructure at the fibril/matrix interface in HDPE matrices reinforced by PA12 fibrils with unidirectional alignment. In the as-prepared MFC (images *a* and *b*) the polyamide reinforcements form oriented crystalline fibrils with core−shell morphology. The long spacings of the PA12 core are between 110 and 120 Å for samples without and with YP, respectively. The core comprises α-PA12 and γ-PA12 polymorphs, whose fractions depend on the compatibilizer content. The HDPE phase is either isotropic (in the bulk matrix) or oriented (the TCL shell of the fibrils). The chain axes of the PA12 in the core and of the PE in the TCL coincide. The long spacings of the isotropic HDPE are smaller than those of the oriented one, typically varying in the ranges of 210−220 Å and 220−235 Å, respectively. In the noncompatibilized samples, the oriented HDPE fraction is present in both equatorial and meridional directions, the latter being with slightly larger long spacings (Table 3). This is an indication for lateral correlation between oriented lamellae forming and incipient lattice structure. In the compatibilized MFC, where chemical bonds are supposed to exist between the N atoms of the PA12 core and the MAH moieties of the transcrystalline polyethylene of YP, joining the respective amorphous regions, no such lateral correlation was registered. In the presence of YP, the TCL is probably reacher in LLDPE oriented molecules being more branched and with lower molecular weight as compared to the matrix HDPE (Table 1).

In the MFC samples after recrystallization of the matrix at 160 °C (Figure 15 c, d) lateral correlation in the TCL polyethylene develops independently of the YP presence. It should be noted that the chain axes of HDPE and PA12 macromoelcules continue to coincide. Similar recrystallization experiments with HDPE/PA6/YP MFC showed that in these systems the compatibilized samples do not develop lateral correlation.[17] This fact can be related with the decreased capability of PA12 to react with the MAH functionality of the LLDPE from YP leading to weaker adhesion at the fibril/matrix interface commented above. Such a supposition was confrimed in our recent real-time SAXS-straining experiments with HDPE/PA6 and HDPE/PA12 oriented precursors for MFC.[42]

## Summary

- The fibrilar morphology of the PA12 reinforcements in the MFC was proved by electron microscopy and synchrotron X-ray methods. As function of the composition, the fibrils diameters varied between 500 and 1250 nm and their length between 11 and 53 $\mu$m, the apparent aspect ratios being between 23 and 83.
- Along with the usual PA12 γ-polymorph, considerable amounts of the α-polymorph were detected in the reinforcing fibrils by 2D WAXS methods. The γ/α form ratio was dependent on the compatibilizer concentration, being up to 2/1 in the noncompatibilized MFC and 1/4 for the compatibilized samples.
- The presence of PE TCL was proved at the fiber−matrix interface with the lamellae being aligned along the PA12 fibers with some lateral correlation depending on the YP content. In all cases the chain directions of the oriented PE and PA12 coincided.
- On the basis of data from WAXS and SEM analyses, the thickness of the polyethylene TCL was calculated. It varied between 43 and 96 nm, depending on the PA12 and compatibilizer content. The real aspect ratio of the PA12 fiber was found to be ca. 100 for the noncompatibilized samples and between 22 and 73 for the compatibilized ones. Idealized models for the structure of the HDPE/PA12/YP UDP MFC were proposed.

**Acknowledgment.** The authors gratefully acknowledge the financial support of the European Commission, Contract Grant Number HPRI-CT-2001-00140, and of HASYLAB at DESY (Grant Number II-07-011 EC). N.D is grateful to Fundação para a Ciência e Tecnologia for supporting her research by Grants SFRH/BD/13435/2003 and SFRH/BPD/45252/2008.

## References and Notes


(1) Schwartz, M. *Composite Materials Handbook*; McGraw-Hill: New York, 1984; Chapter 1, p 23.
(2) Evstatiev, M.; Fakirov, S. *Polymer* **1992**, *33*, 877–880.
(3) Evstatiev, M.; Fakirov, S.; Schultz, J. M. *Polymer* **1993**, *34*, 4669–4679.
(4) Fakirov, S.; Evstatiev, M.; Friedrich, K. In *Handbook of Thermoplastic Polyesters*; Fakirov, S., Ed., Wiley-VCH: Weinheim, Germany, 2002; pp 1093−1132.
(5) Schaefer, D. W.; Justice, R. S. *Macromolecules* **2007**, *40*, 8501–9517.
(6) Denchev, Z.; Dencheva, N. *Polym. Int*. **2008**, *57*, 11–22.
(7) Fakirov, S.; Bhattacharyya, D.; Shields, R. J. *Colloids Surf. A: Physcochem. Eng. Asp*. **2008**, *313−314*, 2–8.
(8) Shields, R. J.; Bhattacharyya, D.; Fakirov, S. *J. Mater. Sci*. **2008**, *43*, 6758–6770.
(9) Li, Z. M.; Xie, B. H.; Huang, R.; Fang, X. P.; Yang, M. B. *Polym. Eng. Sci*. **2004**, *44*, 2165–2173.
(10) Friedrich, K.; Evstatiev, M.; Fakirov, S.; Evstatiev, O.; Ishii, M.; Harrass, M. *Compos. Sci. Technol*. **2005**, *65*, 107–116.
(11) Li, Z. M.; Li, B. L K.; Shen, Z.; Yang, W.; Huang, R.; Yang, M. B. *Macromol. Rapid Commun*. **2004**, *25*, 553–558.
(12) Fuchs, C.; Bhattacharyya, D.; Fakirov, S. *Compos. Sci. Technol*. **2006**, *66*, 3161–3171.
(13) Fakirov, S.; Kamo, H.; Estatiev, M.; Friedrich, K. *J. Macromol. Sci.—Part B Phys*. **2005**, *B43*, 775–89.
(14) Denchev, Z.; Oliveira, M J.; Carneiro, O. S. *J. Macromol. Sci.—Phys*. **2004**, *B43*, 143–162.
(15) Denchev, Z.; Oliveira, M J.; Mano, J F.; Viana, J. C.; Funari, S. S. *J. Macromol. Sci.—Phys*. **2004**, *B43*, 163–76.
(16) Dencheva, N.; Oliveira, M. J.; Carneiro, O. S.; Nunes, T. G.; Denchev, Z. *Mater. Sci. Forum* **2008**, *587−588*, 515–519.
(17) Dencheva, N.; Oliveira, M. J.; Carneiro, O. S.; Pouzada, A. S.; Denchev, Z. *J. Appl. Polym. Sci*. **2010**, *115* (5), 2918–2932.
(18) Quan, H.; Li, Z.- M.; Yang, M. B.; Huang, R. *Compos. Sci. Technol*. **2005**, *65*, 999–1021.
(19) Nuriel, H.; Klein, N.; Marom, G. *Compos. Sci. Technol*. **1999**, *59*, 1685–1690.
(20) Li, Z. M.; Yang, W.; Li, L. B.; Xie, B. H.; Huang, R.; Yang, M. B. *J. Polym. Sci., Part B: Polym. Phys*. **2004**, *42*, 374–385.
(21) Li, Z. M.; Li, L. B.; Shen, K, Z.; Yang, M. B.; Huang, R. *J. Polym. Sci., Part B: Polym. Phys*. **2004**, *42*, 4095–4106.
(22) Friedrich, K.; Ueda, E.; Kamo, H.; Evstatiev, M.; Krasteva, B.; Fakirov, S. *J. Mater. Sci*. **2002**, *37*, 4299–4305.
(23) Sapoundjieva, D.; Denchev, Z.; Evstatiev, M.; Fakirov, S.; Stribeck, N.; Stamm, M. *J. Mater. Sci*. **1999**, *34*, 3063–3066.
(24) Fakirov, S.; Stribeck, N.; Apostolov, A. A.; Denchev, Z.; Krasteva, B.; Evstatiev, M.; Friedrich, K. *J. Macromol. Sci.—Phys*. **2001**, *40*, 935–957.
(25) Saiello, S.; Kenny, J.; Nicolais, L. *J. Mater. Sci*. **1990**, *25*, 3493–3496.
(26) Dencheva, N.; Denchev, Z.; Oliveira, M. J.; Nunes, T. G.; Funari, S. S. *J. Appl. Polym. Sci*. **2008**, *109*, 288–302.
(27) Dencheva, N.; Nunes, T.; Oliveira, M. J.; Denchev, Z. *J. Polym. Sci., Part B: Polym. Phys*. **2005**, *43*, 3720–3733.
(28) Plass, M.; Streck, R.; Nieto, J.; Siesler, H. W. *Macromol. Symp*. **2008**, *265*, 166–177.
(29) Ajji, A.; Zhang, X.; Elkoun, S. *Polym. Eng. Sci*. **2006**, *46*, 1182–1189.
(30) Yang, L.; Zhang, F.; Endo, T.; Hirotsu, T. *Macromolecules* **2003**, *36*, 4709–4718.
(31) Mehrabzadeh, M.; Hossein, N K. *J. Appl. Polym. Sci*. **1999**, *72*, 1257–1265.
(32) Mehrabzadeh, M.; Kasaei, S.; Khosravi, M. *J. Appl. Polym. Sci*. **1998**, *70*, 1–5.
(33) Mehrabzadeh, M.; Kamal, M. R.; Quintanar, G. *Iran Polym. J*. **2009**, *18*, 833–842.
(34) van Duin, M.; Aussems, M.; Borggreve, R. J. M. *J. Polym. Sci., Part A: Polym. Chem*. **1998**, *36*, 179–188.
(35) Thomas, S.; Groeninckx, G. *Polymer* **1999**, *40*, 5799–5819.
(36) Fakirov, S.; Bhattacharyya, D.; Lin, R. J. T.; Fuchs, C.; Friedrich, K. *J. Macromol. Sci., Part B: Phys*. **2007**, *46*, 183–194.
(37) Perilla, J. E.; Jana, S. C. *Polym. Eng. Sci*. **2004**, *44*, 2254–2265.
(38) Software developed by Stonybrook Technology and Applied Research Inc.: New York.
(39) Nogales, A.; Hsiao, B. S.; Somani, R. H.; Srinivas, S.; Tsou, A. H.; Balta-Calleja, F. J.; Ezquerra, T. A. *Polymer* **2001**, *42*, 5247–5256.
(40) Somani, R. H.; Hsiao, B. S.; Nogales, A.; Srinivas, S.; Tsou, A. H.; Sics, I.; Baltá-Calleja, F. J.; Ezquerra, T. A. *Macromolecules* **2000**, *33*, 9385–9394.
(41) Stribeck, N. *X-Ray Scattering of Soft Matter*; Springer Verlag: Berlin and Heidelberg, Germany, 2007; Chapter 1, p 8.
(42) Denchev, Z.; Dencheva, N.; Funari, S. S.; Motovilin, M.; Schubert, T.; Stribeck, N. *J. Polym. Sci.: Part B: Polym. Phys*. **2010**, *48*, 237–250.